The Astrophysical Journal, 693:1686–1695, 2009 March 10 doi:10.1088/0004-637X/693/2/1686

EXPLORING THE DISK–JET CONNECTION FROM THE PROPERTIES OF NARROW-LINE REGIONS IN POWERFUL YOUNG RADIO-LOUD ACTIVE GALACTIC NUCLEI

Nozomu Kawakatu[1], Tohru Nagao[2], and Jong-Hak Woo[3,4]
[1] National Astronomical Observatory of Japan, 2-21-1 Osawa, Mitaka, Tokyo 181-8588, Japan; kawakatu@th.nao.ac.jp
[2] Department of Physics, Graduate School of Science and Engineering, Ehime University, 2-5 Bunkyo-cho, Matsuyama 790-8577, Japan
[3] Physics and Astronomy Department, University of California, Los Angeles, CA 90095-1547, USA
Received 2008 November 2; accepted 2008 December 9; published 2009 March 10

ABSTRACT

We investigate the optical emission-line flux ratios of narrow-line regions in order to determine whether the formation of active galactic nucleus (AGN) jets requires specific accretion conditions. We find that bright compact radio galaxies, which are powerful radio galaxies in the early stage of the jet activity, exhibit systematically larger flux ratios of [O I]λ6300/[O III]λ5007 and smaller flux ratios of [O III]λ5007/[O III]λ4363 than radio-quiet (RQ) Seyfert 2 galaxies. Comparing the observed line ratios with photoionization models, it is found that the difference in the flux ratio of low- to high-ionization lines (e.g., [O I]λ6300/[O III]λ5007) can be well understood by the difference in the spectral energy distribution (SED) of ionizing sources. Powerful young radio-loud (YRL) AGNs favor SED without a strong big blue bump (BBB), i.e., a radiatively inefficient accretion flow (RIAF), while RQ AGNs are consistent with the models adopting SED with a strong BBB, i.e., a geometrically thin, optically thick disk. These findings imply that the formation of powerful AGN jets requires the accretion disk with harder ionizing SED (i.e., an RIAF). We discuss the obscuring structure of YRL AGNs as a plausible origin of the difference in flux ratios of [O III]λ5007/[O III]λ4363.

Key words: accretion, accretion disks – galaxies: active – galaxies: jets

Online-only material: color figures

1. INTRODUCTION

The formation of relativistic jets is one of the fundamental issues in active galactic nuclei (AGNs) physics. The question how the jets form is relevant to supermassive black hole (BH) cases as well as X-ray binaries (XRBs; see reviews by Fender et al. 2003). Thanks to their short dynamical timescale, XRBs in various states have been observed in detail, and it is found that individual sources occupy particular accretion state with various X-ray luminosity (e.g., Fender et al. 2004; Remillard & McClintock 2006). These observations suggested that at low luminosity (i.e., the low mass accretion rate) the jet power is a monotonic function of the accretion luminosity. On the other hand, the jet power may change abruptly by a large factor, following transitions between the soft state (a spectra characterized by the black body components) and hard state (a spectra characterized by the power-law components) at high luminosity (i.e., the high mass accretion rate). By analogy to XRBs, it is expected that the power of AGN jets also depends on the mass accretion rates in a similar way. For example, Rawlings & Saunders (1991) found that for the extended radio galaxies whose projected linear size (LS) is larger than 10 kpc the jet power is proportional to the optical narrow-line luminosity of NLRs which are photoionized by the nuclear continuum radiation (see also Willott et al. 1999). Ghisellini & Celotti (2001) claimed that the less powerful radio galaxies such as Fanaroff–Riley type I radio galaxies (FR Is) exhibit the low accretion rate, while the powerful radio galaxies such as Fanaroff–Riley type II radio galaxies (FR IIs) show the high accretion rate. This work is consistent with a scenario (e.g., Marchesini et al. 2004; Wold et al. 2007) that FR Is have a radiatively inefficient accretion disk (RIAF, e.g., Narayan & Yi 1995), while FR IIs have a standard accretion disk (e.g., Shakura & Sunyaev 1973).

In investigating the disk–jet connection in AGNs, however, we should keep in mind the relatively longer lifetime of the extended radio sources, i.e., FR Is and FR IIs. The reasons are as follows. The timescale of the transition to the different physical states of the accretion disk is $\Delta t(\mathrm{XRBs}) \approx 10^{-2}$ to 10^{-1} yr (a few days to a few weeks change) for XRBs (e.g., Fender et al. 2004). Assuming $M_{\mathrm{BH}}(\mathrm{XRBs}) = 10 M_{\odot}$ and $M_{\mathrm{BH}}(\mathrm{AGNs}) = 10^{8} M_{\odot}$, the transition timescale for AGNs is $\Delta t(\mathrm{AGNs}) \approx 10^{5-6}$ yr because of $\Delta t \propto M_{\mathrm{BH}}$. Thus, the physical states of the accretion disk may change in less than the typical age of extended radio galaxies, i.e., $t_{\mathrm{age}} \approx 10^{7-8}$ yr (e.g., Parma et al. 1999; Bird et al. 2008). In other words, the observed relation between the jet power and the accretion power for the extended radio galaxies may not be proving the direct disk–jet connection in AGNs. Thus, in order to investigate the disk–jet connection in AGNs more directly, it is essential to examine the physical states of the accretion disk in younger radio galaxies.

The young and compact radio galaxies such as compact symmetric objects (CSOs; LS $<$ 1 kpc) and medium-size symmetric objects (MSOs; LS = 1–10 kpc) have been discovered by several authors (e.g., Wilkinson et al. 1994; Fanti et al. 1995; Readhead et al. 1996). Among these compact radio sources, the bright objects show the FR II-like morphology along with hot spots (reverse shocks), which are considered to be a signature of supersonic expansions (Owsianik et al. 1998; Taylor et al. 2000; Tschager et al. 2000; Giroletti et al. 2003; Polatidis & Conway 2003; Gugliucci et al. 2005, 2007; Nagai et al. 2006; Luo et al. 2007). In contrast, the faint compact radio sources do not show hot spots (e.g., Kunert-Bajraszwska et al. 2005; Giroletti 2007) and some of them show the FR I-like morphology (Giroletti 2007). Since the age of CSOs and MSOs is less than $\sim 10^{5}$ yr, they are recognized as newly born young AGN jets

[4] Hubble Fellow.

Table 1
Properties of Powerful YRL AGNs

Name (1)	z (2)	log $P_{5\,\mathrm{GHz}}$ (W Hz^{-1}) (3)	Size (kpc) (4)	log $L_{[\mathrm{O\ III}]}$ (erg s^{-1}) (5)	References (6)
0023–26	0.322	27.0	4.06	···	1
0316+413 (3C 84)	0.017	25.1	4.6×10^{-3}	39.9	3,5
0345+337 (3C 93.1)	0.244	26.0	4.06	40.6	2,3
0404+769 (4C 76.03)	0.598	27.4	0.86	41.9	2,4
0518+165 (3C 138)	0.760	27.8	3.94	44.1	2
0605+480 (3C 153)	0.277	25.7	13.1	41.7	3,5
0710+439	0.518	27.1	0.14	42.4	2,4
0954+658	0.899	26.4	~ 1	43.1	4,6
1031+567	0.459	26.9	0.21	41.6	2,4
1306–09	0.464	27.1	2.72	···	1
1328+307 (3C 286)	0.849	28.2	22.0	44.3	2,3
1345+125 (4C 12.50)	0.122	26.0	0.16	43.0	2,3
1358+624 (4C 62.22)	0.429	26.9	0.35	41.8	2
1443+77 (3C 303.1)	0.267	26.0	6.22	42.9	2,3
1634+628 (3C 343)	0.988	27.7	1.45	···	2
1637+626 (3C 343.1)	0.750	27.4	1.57	43.3	2,3
1807+698 (3C 371)	0.050	25.0	~ 1	40.7	3,6
1934–63	0.183	26.7	0.17	···	1
2342+821	0.735	27.4	1.17	43.1	2,4
2352+495	0.237	26.3	0.17	41.3	2,4

Notes. All quantities are calculated assuming $H_0 = 75\mathrm{kms}^{-1}\mathrm{Mpc}^{-1}$ and $q_0 = 0$. Column 1: object name. Column 2: redshift. Column 3: log of radio power at 5 GHz. Column 4: linear size of the radio jets. Column 5: log of [O III]λ5007 luminosity.
References. (1) Tadhunter et al. (1993); (2) O'Dea (1998); (3) Gelderman & Whittle (1994); (4) Lawrence et al. (1996); (5) Kawakatu et al. (2008); (6) Lister et al. (2001).

(e.g., Fanti et al. 1995; Readhead et al. 1996; O'Dea & Baum 1997; Stanghellini et al. 1999; Snellen et al. 2000; Dallacasa et al. 2000; Orienti et al. 2007). Thus, CSOs and MSOs are adequate targets to examine the disk–jet connection in AGNs since the time lag between the optical and radio activity is relatively small ($\Delta t(\mathrm{AGNs}) \lesssim 10^{5-6}$ yr). In this paper, we will use bright CSOs and MSOs (hereafter powerful young radio-loud, YRL, AGNs) to investigate the disk–jet connection in AGNs.

In order to probe whether the formation of AGN jets requires any specific accretion conditions, it is essential to determine the physical states of the accretion disk of powerful YRL AGNs. To this end, it can be useful to examine a systematic difference in the spectral energy distributions (SEDs) produced by accretion disks of powerful YRL AGNs and radio-quiet (RQ) AGNs. However, it is challenging to derive the intrinsic SEDs of powerful YRL AGNs from the hard X-ray observations, because of the contamination of AGN jets and the obscuration of the accretion disk by the dusty torus. Alternatively, the optical emission-line diagnostics of narrow-line region (NLR) can be used to distinguish the physical states of the accretion disk, since the NLR is thought to be photoionized by the nuclear radiation for RQ Seyfert galaxies (e.g., Yee 1980; Shuder & Osterbrock 1981; Evans et al. 1999) and even for extended radio galaxies (e.g., Villar-Martin et al. 1997; Nagao et al. 2006). However, very little is currently known about the optical emission-line properties of powerful YRL AGNs. By examining the difference of optical line ratios between powerful YRL AGNs and the extended radio galaxies, Morganti et al. (1997) found that powerful YRL AGNs show the characteristics very similar to that of extended radio galaxies. However, it is not clear how the physical state of accretion disks (especially SEDs of accretion disks) is different between the powerful YRL AGNs and the RQ AGNs. Answering this question will provide crucial information on the disk–jet connection in AGNs.

The main goal of this paper is to investigate whether there is the difference in SEDs between the powerful YRL AGNs and Seyfert 2 galaxies (i.e., RQ AGNs), by utilizing the optical emission-line diagnostics of NLRs. We collected samples of powerful YRL AGNs and RQ AGNs (Section 2), and generated various photoionization models with different input SEDs (Section 3). In Section 4, we compared the observational data with models. On the basis of our findings, discussion on accretion conditions for the formation of powerful AGN jets is presented in Section 5, and conclusions follow in Section 6.

2. DATA COMPILATION

We focus on the properties of ionized gas in NLRs for powerful YRL AGNs to investigate the disk–jet connection. To reduce possible inclination effects, it is important to compare AGNs with the same optical type, since the optical narrow emission-line ratios are often affected by the geometrical effects (e.g., Murayama & Taniguchi 1998; Schmitt 1998; Nagao et al. 2000, 2001c). Out of 219 radio galaxies available in the literature, we compiled 32 YRL AGNs (20 narrow-line AGNs and 12 broad-line AGNs) with the optical spectra, from which the stellar continuum is subtracted, and high radio luminosity, log $P_{5\,\mathrm{GHz}} > 25.0$ W Hz^{-1}, using papers by Pearson & Readhead (1988), Tadhunter et al. (1993), and O'Dea (1998). Since only few broad-line YRL AGNs have the detected emission lines (e.g., [O I]λ6300 line, [O II]λ3727, and [O II]λ5007) which are essential for our study, we finally selected 20 *narrow-line* YRL AGNs with these lines. In other words, the YRL AGN sample consists only of radio galaxies. The properties of powerful YRL AGNs are presented in Table 1. The mean projected linear size of selected radio sources is 3.2 kpc, which is small enough to discuss the disk–jets connection in AGNs (see Section 1). The average radio power at

Table 2
Emission-Line Ratios Relative to Hβ Flux

Name	[O II] λ3727	[Ne III] λ3869	[O III] λ4363	[O III] λ5007	[O I] λ6300	[S II] λ6716	[S II] λ6731	References
(1)	(2)	(3)	(4)	(5)	(6)	(7)	(8)	(9)
0023–26	4.90	0.51	0.10	3.40	2.70	2.48	3.10	1
0316+413	2.95	0.92	0.38	10.9	6.61	3.37	2.67	3
0345+337	···	···	···	8.33	2.00	···	···	2
0404+769	···	0.33	···	3.66	···	···	···	3
0518+165	···	···	···	0.93	···	···	···	2
0605+480	5.25	···	···	4.74	2.26	3.17	2.71	3
0710+439	2.54	0.44	0.28	6.10	1.33	···	···	3
0954+658	0.45	0.47	0.33	7.48	···	···	···	3
1031+567	3.16	0.98	···	7.20	5.80	···	···	3
1306–09	4.64	0.60	0.06	3.57	···	···	···	1
1328+307	0.48	0.57	0.39	4.34	···	···	···	2
1345+125	2.19	1.06	0.38	6.25	0.94	···	···	2
1358+624	2.49	0.78	0.10	8.69	5.61	3.49	5.04	3
1443+77	4.58	0.50	···	9.00	···	···	···	4
1634+628	2.06	1.08	0.18	···	···	···	···	3
1637+626	···	···	···	6.33	···	···	···	2
1807+698	1.10	···	···	3.66	2.34	1.06	2.01	3
1934–63	3.12	1.44	0.26	7.21	···	···	···	1
2342+821	0.94	0.59	···	9.98	···	···	···	3
2352+495	3.21	0.80	···	8.56	3.88	3.25	3.01	3

Notes. Column 1: object name. Columns 2–8: emission-line ratios relative to Hβ flux.

References. (1) Morganti et al. (1997); (2) Gelderman & Whittle (1994); (3) Lawrence et al. (1996); (4) Labiano et al. (2005).

5 GHz, log $P_{5\,\mathrm{GHz}}$ is $\approx$ 27.0 W Hz^{-1}, comparable to powerful extended radio galaxies (Laing et al. 1983). Note that the radio power of the faint YRL AGNs, excluded from our sample, is log $P_{5\,\mathrm{GHz}} \leqslant 25.0$ W Hz^{-1} (e.g., Giroletti 2007). We use only the forbidden lines to avoid the difficulty of separating the broad component and the narrow component of the recombination lines (e.g., Hα and Hβ lines). Then, we compiled the flux ratios of forbidden emission lines from the literature (Table 2). The typical errors of each line are ≈10%–30%.

To compare with narrow-line YRL AGNs, we selected a sample of RQ Seyfert 2 galaxies from the Sloan Digital Sky Survey (SDSS; York et al. 2000) archive, using the emission-line flux catalog made by the MPA/JHU group (Kauffmann et al. 2003). We selected 624 RQ Seyferts, of which First Images of the Radio Sky at Twenty cm (FIRST) flux is lower than 1 mJy and optical emission-line fluxes are well measured from high signal-to-noise ratio (greater than 10) SDSS spectra.

In this paper, we do not evaluate the amount of extinction of host galaxies based on the Balmer decrement method (e.g., Osterbrock 1989), since for only few sources in the powerful YRL AGN sample detected were both the narrow Hα and Hβ lines. The data presented in Table 2 are not corrected for Galactic extinction. The effect of dust extinction on our results will be discussed in Section 4.1.

3. PHOTOIONIZATION MODEL

To characterize SEDs produced by the accretion disk in powerful YRL AGNs, we will compare emission-line properties with photoionization models. We will examine whether there is a systematic difference in SEDs from accretion disks between the powerful YRL AGNs and the RQ AGNs. The continuum radiation from the accretion disk photoionizes the NLR, hence, the difference in the SED can be related to the difference in the physical states of the NLR. Then, we compare the observed flux ratios with photoionization model calculations, using the publicly available code CLOUDY, version 06.02c (Ferland et al. 1998).

The method of our calculations is based on solving the equations of statistical equilibrium, the ionization and thermal equilibrium through gas clouds as a function of depth. Then, we obtain the ionization structure of gas in NLRs and the volume emissivity of the forbidden emission lines (i.e., [O I]λ6300, [O II]λ3727, [S II]λ6717+6731, [O III]λ5007, and [Ne III]λ3869). Here we briefly describe the adopted parameterizations. We assume uniform-density gas clouds with a plane-parallel geometry. The parameters for the calculations are (1) the hydrogen density (n_{H}), (2) the ionization parameter ($U = Q(\mathrm{H})/4\pi cr^2 n_{\mathrm{H}}$, where $Q(\mathrm{H})$ is the number of the ionizing photons emitted by AGNs per second), which is defined as the ratio of the ionizing density to the hydrogen density, (3) the chemical composition of the gas, and (4) the shape of SEDs of the input continuum radiation. While the gas metallicity is assumed to be solar (Grevesse & Sauval 1998; Holweger 2001), we carry out a series of model runs covering various density and ionization parameters: $10^2\,\mathrm{cm}^{-3} \leqslant n_{\mathrm{H}} \leqslant 10^5\,\mathrm{cm}^{-3}$ and $10^{-4.0} \leqslant U \leqslant 10^{-1.5}$.

For the input continuum radiation, we consider two types of SEDs. One is a typical SED produced by a standard accretion disk (Shakura & Sunyaev 1973), which is characterized by a strong big blue bump (BBB) in the wavelength range of UV to soft X-ray. As a template of this type of SED (hereafter SED with BBB), we adopt the empirical expression using the following function (see Ferland 1997; Nagao et al. 2001a):

$$f_\nu = \nu^{\alpha_{\mathrm{UV}}} \exp\left(-\frac{h\nu}{kT_{\mathrm{BB}}}\right) \exp\left(-\frac{kT_{\mathrm{IR}}}{h\nu}\right) + a\nu^{\alpha_{\mathrm{x}}}, \qquad (1)$$

where the infrared cutoff of the BBB component, $kT_{\mathrm{IR}} = 0.01$ ryd (1ryd = 13.6 eV), the characteristic temperature of the BBB, $T_{\mathrm{BB}} = 4.9 \times 10^5$ K, the slope of the low-energy side of the BBB, $\alpha_{\mathrm{UV}} = -0.5$, the UV to X-ray spectral index, $\alpha_{\mathrm{ox}} = -1.35$, and the slope of the X-ray power-law continuum, $\alpha_{\mathrm{x}} = -0.85$, which are typical values of Seyfert galaxies (see Nagao et al. 2001a for more details). Since the characteristic temperature of the BBB in some extreme AGNs, e.g., narrow-line Seyfert 1 galaxies, can reach at $T_{\mathrm{BB}} \approx 10^6$ K, we will discuss the effects of changing T_{BB} on the line flux ratios. Note that the parameter a in Equation (1) is determined from the adopted value of α_{ox}. The last term in Equation (1) is set to zero below 1.36 eV, and the continuum is assumed to fall off as ν^{-3} above 100 keV.

The other kind of SED is a typical SED produced by an RIAF, which is expected to show a power law with no strong BBB as shown by various works (e.g., Narayan & Yi 1995; Chen et al. 1997; Narayan et al. 1997; Manmoto et al. 1997; Kurpiewski & Jaroszynski 1999; Quataert & Narayan 1999; Manmoto 2000; Kino et al. 2000; Ohsuga et al. 2005; Yuan et al. 2008). We adopt here the SED model presented by Kurpiewski & Jaroszynski (1999) as the template for SEDs of RIAF (hereafter SED without BBB). This SED can be expressed by a single power-law continuum in the range of 10^{12} Hz to 10^{20} Hz, with the exponential cutoffs at 10^{-4} ryd and 10^4 ryd. We choose the photon index of $\alpha_{\mathrm{PL}} = 0.89$ ($f_\nu = \nu^{-\alpha_{\mathrm{PL}}}$), as predicted for the case of a nonrotating BH. Since there are various shapes of the calculated SED for an RIAF (i.e., various α_{PL}), we will check the effect of altering α_{PL} in the wide range of $0.78 < \alpha_{\mathrm{PL}} < 1.0$.

Using these two SED templates for a standard disk and RIAF, respectively (see Figure 3 in Nagao et al. 2002), we calculate emission-line flux ratios using CLOUDY. These simple SED templates can be used to elucidate the effect of the presence or absence of the BBB component, which is the main difference in the SED between a standard disk and RIAF. Note that these templates might be too simple to generate accurate narrow emission-line fluxes in AGNs. The calculations are stopped when the temperature falls below 3000 K, where the gas does not contribute significantly to the observed optical emission-line spectra.

4. RESULTS

In this section, we compare the photoionization model calculations with observed emission-line properties of powerful YRL AGNs and Seyfert 2 galaxies.

4.1. Comparison With Models With/Without BBB

The emission-line ratio, [O I]λ6300/[O III]λ5007, of the NLR can be used to characterize the SED of accretion disk since the line ratio depends on the shape of SED of the photoionizing source. The harder spectra (without BBB) of optically thin disks create larger ratios [O I]λ6300/[O III]λ5007 due to the following reasons. The mean free path of ionizing photons at higher energies becomes longer, since the cross section for ionization of hydrogen (σ(H)) is given by σ (H) $\propto (\nu/\nu_{\rm L})^{-3}$ for $\nu > \nu_{\rm L}$, where $\nu_{\rm L}$ is the frequency of the Lyman limit. With a flat power-law spectrum ($\alpha_{\rm PL} \lesssim 1$), a relatively large number of photons are available at higher energies even after the photons near the Lyman limit are all absorbed around the ionization front. Then, the higher energy photons can reach at larger radii from the ionization source, hence, the extended partially ionized region can be formed. Furthermore, the low-ionization emission arises in the extended partially ionized region rather than the fully ionized region where the abundance of neutral oxygen is negligible. Therefore, the volume emissivity of low-ionization emission lines (i.e., [O I]λ6300) can be higher at larger radii from the ionization sources, compared to that of high-ionization emission lines (i.e., [O III]λ5007; see Figure 5 of Nagao et al. 2002). Note that the ionization potential of neutral oxygen is nearly identical to that of hydrogen.

Figure 1 represents emission-line ratios ([O I]λ6300/[O III]λ5007 vs. [O II]λ3727/[O III]λ5007) from our model calculations and observations. The horizontal axis ([O II]λ3727/[O III]λ5007) indicates the difference of $n_{\rm H}$ because the critical density of [O II]λ3727 ($n_{\rm H} = 4.5 \times 10^3\,{\rm cm}^{-3}$) is far smaller than that of [O III]λ5007 ($n_{\rm H} = 7.0 \times 10^5\,{\rm cm}^{-3}$). This set is free from the chemical abundance effect. As shown in Figure 1, powerful YRL AGNs have relatively higher [O I]λ6300/[O III]λ5007 than Seyfert 2 galaxies, implying that there is a difference in the shape of ionizing continuum. The observed line ratios were not corrected for both the Galactic extinction or internal extinction of host galaxies. Instead, we indicate by the arrow (upper left in Figure 1) the effect of dust extinction when the dust-extinction correction of $A_{\rm v} = 1.0$ mag is applied, assuming a standard Galactic reddening law (Cardelli et al. 1989). For type 1 AGNs, the dust reddening of NLR emission is small ($A_{\rm v} < 1.0$ mag; e.g., Rodriguez-Ardila et al. 2000). The dust extinction of NLRs for type 2 AGNs is approximately 1.0 mag larger than that for type 1 AGNs (e.g., De Zotti & Gaskell 1985; Dahari & De Robertis 1988).

The models using SED without BBB predict a higher [O I]λ6300/[O III]λ5007 ratio than the models using SED with BBB. The trend of the model prediction coincides with the observations. The line ratios of Seyfert 2 galaxies are consistent with models adopting the SED with BBB in the range of $10^{-3.5} < U < 10^{-3.0}$ and $10^{4.0}\,{\rm cm}^{-3} < n_{\rm H} < 10^{5.0}\,{\rm cm}^{-3}$, while the line ratios of powerful YRL AGNs can be explained by the model adopting the SED without BBB. Note that the derived $n_{\rm H}$ may not reflect the actual number density of narrow-line clouds because of the dust extinction effects. However, the direction of extinction correction is perpendicular to the direction of the difference between powerful YRL AGNs and Seyfert 2 galaxies, indicating that the observed difference is not due to the difference in the degree of the dust extinction between powerful YRL AGNs and Seyfert 2 galaxies.

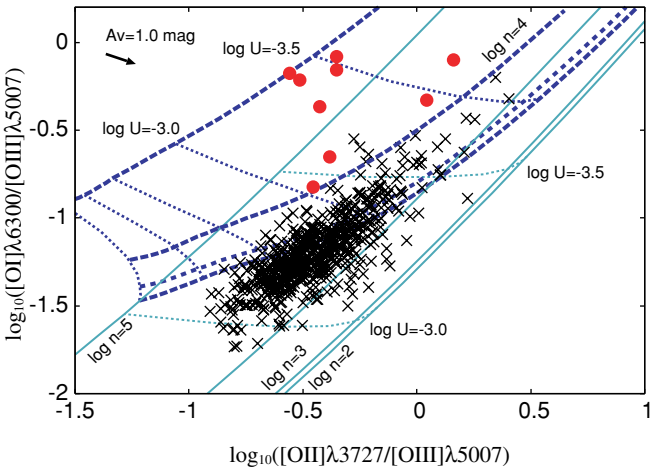

Figure 1. Diagram of [O I]λ6300/[O III]λ5007 vs. [O II]λ3727/[O III]λ5007. The observed line ratios from the literature are presented for powerful YRL AGNs (red circles) and RQ Seyfert 2 galaxies (black crosses). Solid and dashed lines represent our photoionization model calculations using the SED with BBB and the SED without BBB, respectively.

(A color version of this figure is available in the online journal.)

In Figure 2, we present the frequency distributions of log([O I]λ6300/[O III]λ5007) for the powerful YRL AGNs (blue) and Seyfert 2 galaxies (red). The mean value of log([O I]λ6300/[O III]λ5007) for powerful YRL AGNs is -0.36 ± 0.26, while that of log([O I]λ6300/[O III]λ5007) for Seyfert 2 galaxies is -1.17 ± 0.05. The Kolmogorov–Smirnov (K-S) test indicates 10^{-4} probability that the observed frequency distributions of [O I]λ6300/[O III]λ5007 of powerful YRL AGNs and Seyfert 2 galaxies originate from the same underlying population, suggesting that the emission-line ratios of [O I]λ6300/[O III]λ5007 for powerful YRL AGNs are statistically larger than those of Seyfert 2 galaxies.

In Figure 3, we compare the observations with the model predictions in other diagnostic diagrams, i.e., [O I]λ6300/[O III]λ5007 versus [S II]λ6717+6731/[O III]λ5007 and [O I]λ6300/[O III]λ5007 versus [Ne III]λ3869/[O II]λ3727. The physical meaning of these diagrams is the same as Figure 1. Similar to the trend in Figure 1, powerful YRL AGNs and Seyfert 2 galaxies are well separated in these diagnostic diagrams, suggesting that the different line ratios of powerful YRL AGNs can be explained by models with the photoionizing SED without BBB. However, one may doubt that the difference of SED is not a unique solution to explain the observed differences. Thus, we discuss the other possibilities for high [O I]λ6300/[O III]λ5007 ratios in Section 5.1.

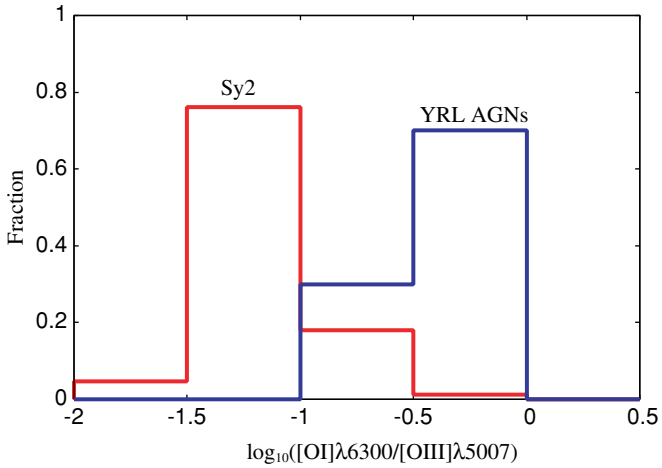

Figure 2. Frequency distributions of emission-line flux ratios [O I]λ6300/[O III]λ5007, for powerful YRL AGNs (red) and Seyfert 2 galaxies (blue).

(A color version of this figure is available in the online journal.)

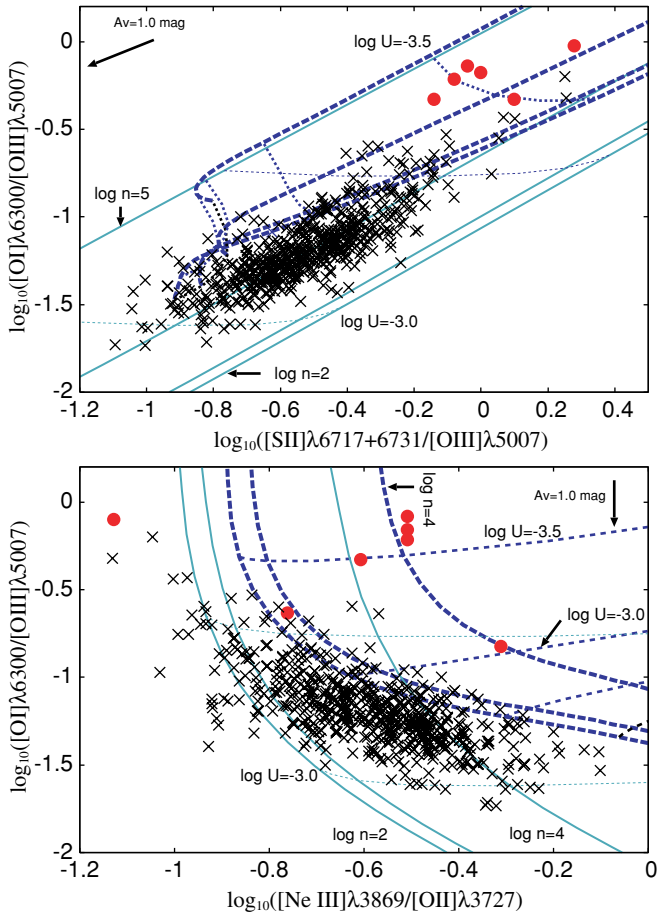

Figure 3. Diagram of [O I]λ6300/[O III]λ5007 vs. [S II]λ6717+6731/[O III]λ5007 (top) and that of [O I]λ6300/[O III]λ5007 vs. [Ne III]λ3869/[O III]λ3727 (bottom). Symbols and lines are the same as Figure 1.

(A color version of this figure is available in the online journal.)

4.2. Dependence on the Model Parameters

Here, we examine the dependence of emission-line ratios on the model input parameters, T_{BB} and α_{PL}. Figure 4 shows the optical emission-line ratios ([O I]λ6300/ [O III]λ5007 and [O II]λ3727/[O III]λ5007) as a function of α_{PL} (left panel) and T_{BB} (right panel), assuming $n_H = 10^4\,cm^{-3}$. We find that at given U the variations of T_{BB} and α_{PL} does not change significantly the line ratios of [O I]λ6300/[O III]λ5007, compared to the effect of the difference in SEDs of ionizing radiation. Since the change of emission-line ratios due to α_{PL} or T_{BB} is relatively small, the effect of changing T_{BB} and α_{PL} cannot account for the observed difference between powerful YRL AGNs and Seyfert 2 galaxies. The effect of both T_{BB} and α does not also change the results shown in Figure 3. Therefore, the difference in the observed emission-line ratios in Figures 1 and 3 is consistent with the idea that the NLR of powerful YRL AGNs is photoionized by SEDs without BBB, while that of the RQ AGNs is photoionized by SEDs with BBB.

4.3. [O III]λ5007/[O III]λ4363

In Figure 5, we investigate [O III]λ5007/[O III]λ4363 line ratios, which is one of the gas temperature indicators (Osterbrock 1989). The line ratio ([O III]λ5007/[O III]λ43 63) of powerful YRL AGNs is smaller than that of Seyfert 2 galaxies. The mean value of log([O III]λ5007/[O III]λ4363) for powerful YRL AGNs is 1.50 ± 0.29, while that for Seyfert 2 galaxies is 2.03 ± 0.16. The frequency distributions of these line ratios for the powerful YRL AGNs (blue) and Seyfert 2 galaxies (red) are presented in Figure 6. The K-S test indicates 10^{-4} probability that the observed frequency distributions of [O III]λ5007/[O III]λ4363 of YRL AGNs and Seyfert 2 galaxies originate in the same underlying population. We will discuss potential physical reasons for smaller [O III]λ5007/[O III]λ4363 of powerful YRL AGNs in Section 5.3.

5. DISCUSSION

5.1. Other Possibilities for High [O I]λ6300/[O III]λ5007 Ratios

We here consider three other plausible possibilities which may explain the observed difference in line ratios.

1. *Shock ionization.* We consider the shock ionization due to the interaction between AGN jets and the clouds in NLRs. The strong low-ionization emission lines such as [O I]λ6300 causes by the shock-heated gas (e.g., Mouri et al. 2000 and references therein) because shocks generate a large partially ionized region in the gas. To investigate whether or not the shock heating by AGN jets is responsible for the difference in the narrow emission-line ratio between powerful YRL AGNs and RQ AGNs, we compare the observed line ratios with shock models in Figure 7. The adopted shock models with/without considering the effect of precursor[5] are presented by Dopita & Sutherland (1995). The shock models predict too small flux ratio of [O I]λ6300/[O III]λ5007, too small flux ratio of [Ne III]λ3869/[O II]λ3727, and too large [O II]λ3727/[O III]λ5007, compared with the observed line ratios of powerful YRL AGNs. To explain all observations (Figures 1 and 3) by shock models, a fine-tuning of model parameters should be required. Thus, these results suggest that the difference in the narrow-line flux ratios of powerful YRL AGNs are not mainly caused by the shock-heated gas in NLRs. However, we should mention that for one of the YRL AGNs in our sample (3C 303.1) the shock ionization cannot be negligible (e.g., Labiano et al. 2005). Note that the NLR properties of powerful YRL AGNs can be explained by the photoionization model (on

[5] This effect is that the unshocked gas is ionized by the radiation emitted by the hot shocked gas.

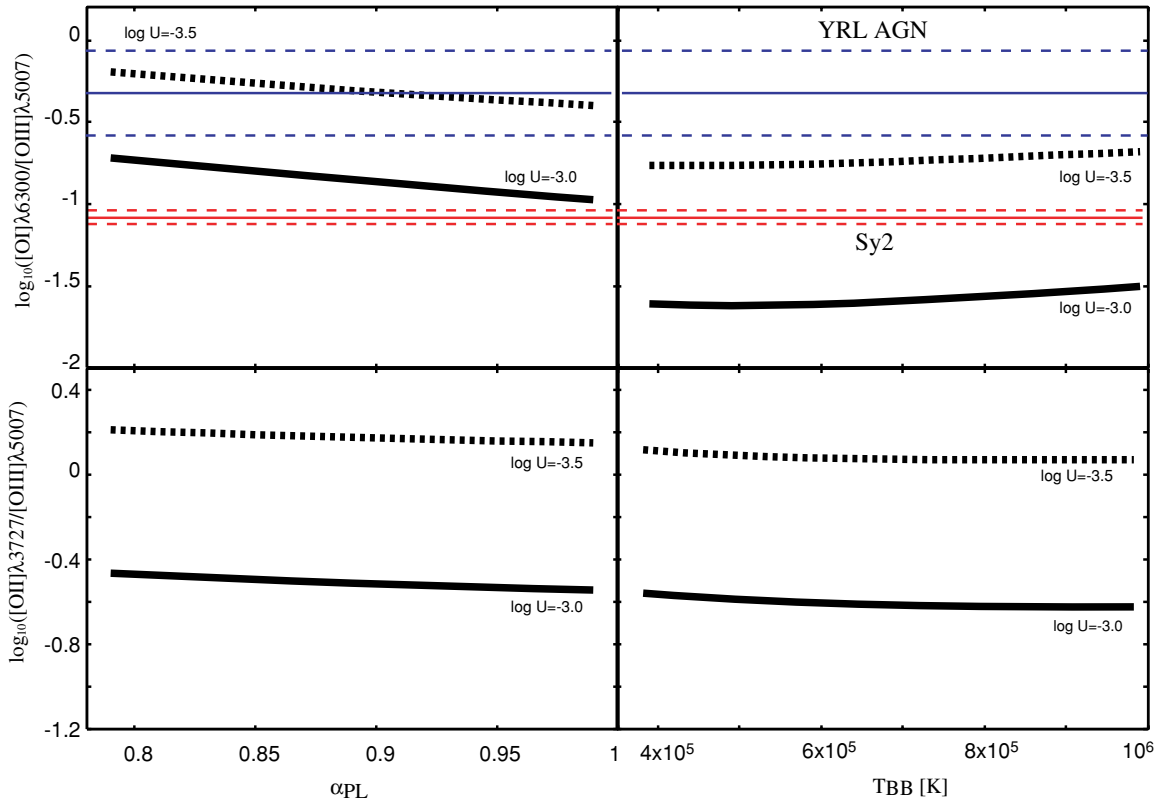

Figure 4. Optical emission-line ratios ([O I]λ6300/[O III]λ5007 and [O II]λ3727/[O III]λ5007) as a function of the power-law index of RIAF-like SEDs, $\alpha_{\rm PL}$ (left), and the characteristic temperature, $T_{\rm BB}$ (right) for a standard accretion disk, assuming $n_{\rm H} = 10^4\,{\rm cm}^{-3}$. The solid lines represent the case of $\log U = -3.0$, while the dotted lines denote that of $\log U = -3.5$. The blue (red) solid line represents the mean value of log([O I]λ6300/[O III]λ5007) for powerful YRL AGNs (Seyfert 2 galaxies). The blue (red) dotted lines correspond to the dispersion of log([O I]λ6300/[O III]λ5007).

(A color version of this figure is available in the online journal.)

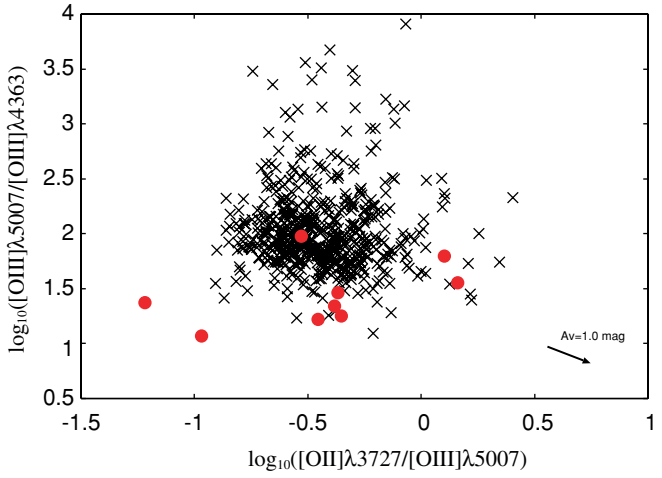

Figure 5. Diagram of [O III]λ5007/[O III]λ4363 vs. [O II]λ3727/[O III]λ5007. Symbols and lines are the same as in Figure 1.

(A color version of this figure is available in the online journal.)

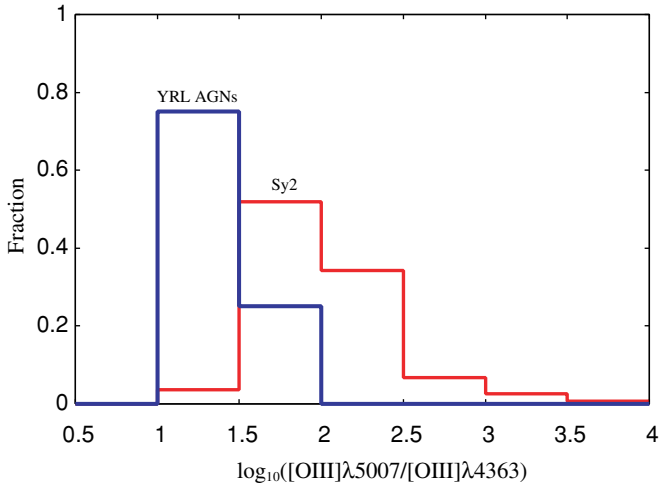

Figure 6. Frequency distributions of the emission-line flux ratios of [O III]λ5007/[O III]λ4363, for powerful YRL AGNs (red) and Seyfert 2 galaxies (blue).

(A color version of this figure is available in the online journal.)

average), in spite of the signature of the strong kinematic interaction with surrounding gas (e.g., Axon et al. 2000; O'Dea et al. 2002; Holt et al. 2008; Labiano 2008).

2. *Gas density.* The systematic difference in the gas density in NLR may cause the different line ratios, because the critical density of [O I]λ6300 transition ($n_{\rm H} = 1.8 \times 10^6\,{\rm cm}^{-3}$) is larger than that of [O III]λ5007 transition ($n_{\rm H} = 7.0 \times 10^5\,{\rm cm}^{-3}$). This possibility can be easily rejected as shown in Figures 1 and 3. At given ionization parameter U, the ratio of [O I]λ6300/[O III]λ5007 does not depend on the gas density, if we employ only the models with SEDs with BBB. This is because both critical densities of [O I]λ6300 transition and [O III]λ5007 transition are higher than the typical gas density of NLRs in AGNs ($10^{2.0}\,{\rm cm}^{-3} \leqslant n_{\rm H} \leqslant 10^{5.0}\,{\rm cm}^{-3}$). This indicates that the observed difference in the flux ratio of [O I]λ6300/[O III]λ5007 is not caused only by a systematic difference in the gas density of NLRs.

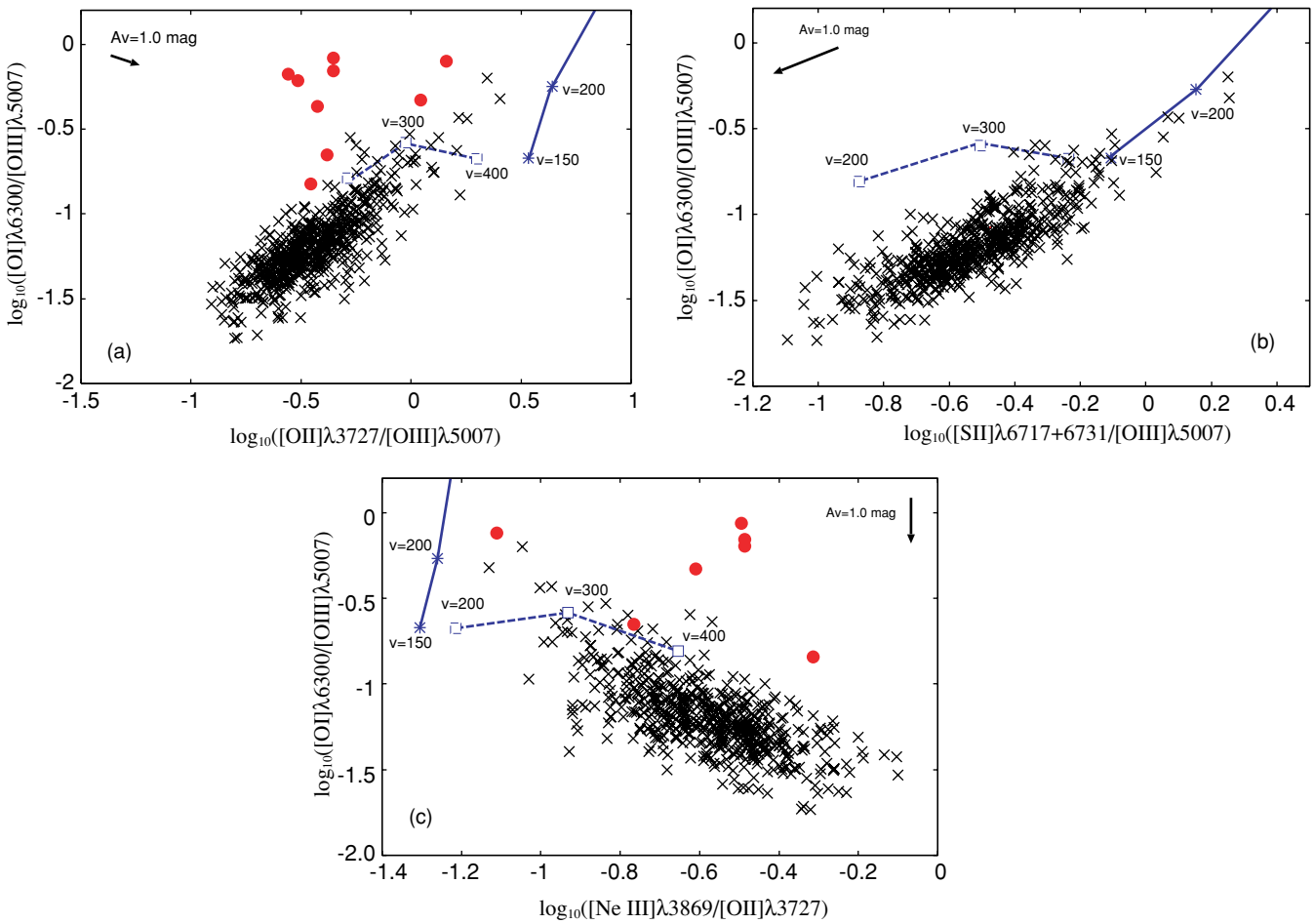

Figure 7. (a) Diagram of [O I]λ6300/[O III]λ5007 vs. [O II]λ3727/[O III]λ5007, (b) diagram of [O I]λ6300/[O III]λ5007 vs. [S II]λ6717+6731/[O III]λ5007, and (c) diagram of [O I]λ6300/[O III]λ5007 vs. [Ne III]λ3869/[O III]λ3727. Predictions of the shock model (Dopita & Sutherland 1995) are represented by blue lines. The blue solid lines denote the pure-shock model ($150\,\mathrm{km\,s^{-1}} \leqslant v_{\rm shock} \leqslant 500\,\mathrm{km\,s^{-1}}$), while the blue dotted lines denote the models considering the effect of precursor ($200\,\mathrm{km\,s^{-1}} \leqslant v_{\rm shock} \leqslant 500\,\mathrm{km\,s^{-1}}$). Chemical composition of solar abundances and the magnetic parameter of $B/\sqrt{n} = 2\mu\mathrm{G\,cm^{2/3}}$ are assumed in these models (see Table 1 in Dopita & Sutherland 1995 for details). Symbols and line are the same as Figure 1.

(A color version of this figure is available in the online journal.)

3. *Ionization parameter.* We consider the difference in the ionization parameter U between powerful YRL AGNs and RQ AGNs. Since the effect of the SED difference and changing the ionization parameter (i.e., the ratio of the ionizing photon density to the hydrogen density) are often degenerated (see Nagao et al. 2002), a systematic difference in the ionization parameter of gas in NLRs between powerful YRL AGNs and RQ AGNs can explain the difference in the emission-line ratios [O I]λ6300/[O III]λ5007 when we fix $n_{\rm H}$. As shown in Figures 1 and 3 (bottom), we find that only different U cannot explain the difference of line ratios between powerful YRL AGNs and RQ AGNs. However, it is possible that the combination of $n_{\rm H}$ and U can reproduce the difference between them even if we assume the SEDs with BBB. If the NLR of powerful YRL AGNs has generally higher $n_{\rm H}$ and lower U than that of Seyfert 2 galaxies, the observed difference can be explained without invoking different shape of photoionizing SEDs. This possibility cannot be completely ruled out from Figures 1 and 3; however, a special fine-tuning of model parameters is required to generate the observed line ratios of powerful YRL AGNs.

The degeneracy of the effect of SED shape and of the ionization parameter is a limitation in interpreting these results. For the future studies, the diagnostic diagram using the flux ratio of [Ar III]λ7136/[O III]λ5007 (e.g., [Ar III]λ7136/[O III]λ5007 vs. [O II]λ3727/[O III]λ5007 and [Ar III]λ7136/[O III]λ5007 vs. [Ne III]λ3727/[O III]λ5007) can be used to determine the ionization parameter, since [Ar III]λ7136/[O III]λ5007 is almost independent of the shape of SED in the range of $U \lesssim 10^{-2.5}$ (Nagao et al. 2002). Thus, it can be better constrained whether the SEDs of YRL AGNs are different from those of Seyfert 2 galaxies. Unfortunately, these lines are not currently available for our sample of YRL AGNs.

5.2. Disk–Jet Connection

In Section 4, we have shown that the powerful YRL AGNs favor SEDs without a strong BBB such as the one expected for RIAFs. On the other hand, it is well known that RIAFs are radiatively inefficient and generate relatively lower Eddington ratios (e.g., Narayan & Yi 1995; Kato et al. 1998).

The advection-dominated solution exists when the mass accretion rate is relatively low as $\dot{M} \leqslant \dot{M}_{\rm max}$. If we assume a fiducial efficiency is $\approx 10\%$ (Frank et al. 1992), the maximum accretion rate is given by $\dot{M}_{\rm max} \approx 3\alpha^2 L_{\rm Edd}/c^2$ at $r < 100 r_{\rm g}$, where $r_{\rm g}$ is the Schwarzschild radius of the central BH, α is the α-viscosity (Shakura & Sunyaev 1973), and $L_{\rm Edd}$ is the Eddington luminosity corresponding to the Thomson scattering. The energy release from an RIAF ($L_{\rm RIAF}$) can be obtained as

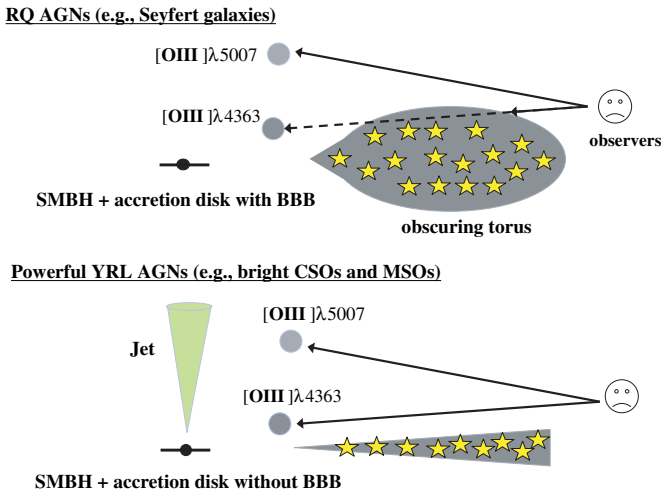

Figure 8. Schematic sketches for the properties of accretion disk and the obscuring materials of the RQ Seyfert 2 galaxies (upper) and the powerful YRL AGNs, i.e., CSOs and MSOs (lower). The light gray circles denote the narrow-line clouds emitting [O III]λ5007 and the dark gray circles represent the narrow-line clouds emitting [O III]λ4363.

(A color version of this figure is available in the online journal.)

$L_{\rm RIAF} \approx 0.1(\dot{M}/\dot{M}_{\rm max})\dot{M}c^2$ (e.g., Kato et al. 1998). According to three-dimensional magneto-hydrodynamic simulations, α is $\alpha \lesssim 0.1$ (e.g., Balbus & Hawley 1991; Machida et al. 2000; Machida & Matsumoto 2003). We here adopt the conservative value as $\alpha = 0.1$ and then the maximum luminosity of an RIAF at $\dot{M} = \dot{M}_{\rm max}$ is given as $L_{\rm RIAF,max} \approx 10^{-3} L_{\rm Edd}$.

Thus, it is necessary to consider whether RIAFs are able to explain the relatively high [O III]λ5007 luminosity (hence, high bolometric luminosity) of powerful YRL AGNs. First, we estimated the bolometric luminosity of powerful YRL AGNs based on the [O III] luminosity. The [O III] luminosity of 16 powerful YRL AGNs were collected from Gelderman & Whittle (1994) and Lawrence et al. (1996); see Table 1. The average [O III] luminosity is $\bar{L}_{[\rm O\,III]} = 10^{42.24\pm1.25}$ erg s^{-1}. To evaluate the bolometric luminosity, we adopt the bolometric correction of low-luminosity AGNs (LLAGNs) whose SEDs can be well expressed by an RIAF model because of the lack of BBB (e.g., Ho 1999), i.e., $L_{\rm bol} \approx 250\, L_{[\rm O\,III]}$ with variance of 0.9 dex (Panessa et al. 2006).[6] Then, the average bolometric luminosity of YRL AGNs, $\bar{L}_{\rm bol,obs} \sim 10^{45}$ erg s^{-1}, is required to produce the observed [O III] line luminosity. This suggests that $\bar{L}_{\rm bol,obs}$ is $\sim 10^{-2}\, L_{\rm Edd}$ for the massive BHs ($M_{\rm BH} = 10^9 M_\odot$). Hence, it seems difficult to explain the bolometric luminosity of powerful YRL AGNs with the RIAF model, because of $L_{\rm RIAF,max} \lesssim 0.1\bar{L}_{\rm bol,obs}$. The combination of emission-line ratios and the bolometric luminosity estimates implies that the physical nature of the accretion disk of YRL AGNs cannot be explained by either the classical steady disk, i.e., a standard disk or an RIAF. It might imply that the relativistic jet occur in a non steady accretion disk.

Interestingly, the physical states of accretion disks in some XRBs (e.g., GX 339–4) associated with relativistic jets are similar to those of YRL AGNs (Homan et al. 2005; Remillard 2005), suggesting the similarity of disk–jet connection in XRBs and AGNs. This similarity may indicate that the formation of relativistic jets requires luminous accretion disk with harder ionizing SED. However, we note that the bolometric luminosity estimated from [O III] luminosity is highly uncertain for both luminous AGNs and LLAGNs without BBB. Thus, it is crucial to reduce the uncertainty of bolometric luminosity by evaluating the bolometric correction using a large sample of broad-line YRL AGNs, which are left in our future works.

[6] $\log(L_{2-10\rm keV}/L_{[\rm O\,III]}) = 1.5 \pm 0.5$ and $\log(L_{\rm bol}/L_{2-10\rm keV}) = 0.9 \pm 0.4$.

5.3. Obscuring Structure in Powerful YRL AGNs

We discuss here why the line ratios, log([O III]λ5007/[O III]λ4363), of powerful YRL AGNs is smaller than that of Seyfert 2 galaxies. As we investigated in Section 4, several optical narrow-line emission ratios ([O I]λ6300/[O III]λ5007, [O II]λ3727/[O III]λ5007, [S II]λ6717+6731/[O III]λ5007, and [Ne III]λ3869/[O II]λ3727) can be well explained by single-zone photoionization models. However, it has been well known that any one-zone model overpredicts the flux ratio of [O III]λ5007/[O III]λ4363 (e.g., Koski & Osterbrock 1976; Heckman 1980; Ferland & Netzer 1983; Rose & Cecil 1983; Keel & Miller 1983; Rose & Tripicco 1984).

By taking high-density gas clouds into account in NLRs, Nagao et al. (2001b) reported that photoionization models can explain low emission-line flux ratios of [O III]λ5007/[O III]λ4363 $\sim$ 10, without including shock effects. This idea is attributed to the fact that the critical density of [O III]λ4363 ($n_{\rm H} = 3.3 \times 10^7 {\rm cm}^{-3}$) is higher than that of [O III]λ5007 ($n_{\rm H} = 7.0 \times 10^5 {\rm cm}^{-3}$). In addition, they suggested that the [O III]λ4363 originates in the dense gas clouds which are located at the inner regions compared with [O III]λ5007, hence, a large fraction of gas clouds emitting [O III]λ4363 line are obscured in type 2 AGNs. This idea is supported by the observations that the line ratios of [O III]λ5007/[O III]λ4363 of Seyfert 2 galaxies are larger than those of Seyfert 1 galaxies (Nagao et al. 2001b). If this is the case, the difference in [O III]λ5007/[O III]λ4363 may reflect the difference in the structure of duty torus, i.e., the difference of the geometrical thickness. We should emphasize that the difference in Figure 5 (also Figure 6) is not related to the inclination effect, because we compare the same optical types of AGNs, i.e., powerful narrow-line YRL AGNs and Seyfert 2 galaxies. Since the ratio [O III]λ5007/[O III]λ4363 of powerful YRL AGNs is lower than that of Seyfert 2 galaxies, the obscuring torus of powerful YRL AGNs may be thinner than that of Seyfert 2 galaxies (see Figure 8). According to a recent coevolution model of the BH growth and the circumnuclear disk (Kawakatu & Wada 2008; see also Wada & Norman 2002), the mass accretion rate onto a central BH driven by the turbulent viscosity is higher as the scale height of circumnuclear disk increases. This is because the angular momentum transfer due to the turbulence is proportional to the scale height. To test our scenario, it is crucial to examine the difference in the structure of obscuring torus, using Atacama Large Millimeter/submillimeter Array (ALMA).

In summary, our findings indicate that the powerful YRL AGNs favor the accretion disk without BBB, surrounded by the geometrically thin obscuring torus, while Seyfert 2 galaxies prefer the accretion disk with BBB, surrounded by the geometrically thick torus (see Figure 8). These results suggest that the formation of the powerful AGN jet is related to the physical states of accretion disks and structure of obscuring materials around the accretion disk.

6. CONCLUSIONS

We examine the optical narrow emission-line flux ratios of NLRs, in order to determine whether the formation of powerful

AGN jets requires specific accretion conditions. A sample of powerful YRL AGNs, which are at the early stage of the jet activity, and RQ Seyfert 2 galaxies are selected. We summarize our main results.

1. Powerful YRL AGNs exhibit larger flux ratios of [O I]λ6300/[O III]λ5007 than RQ Seyfert 2 galaxies. By comparing the observed line ratios with the photoionization model calculations, we find that the difference between powerful YRL AGNs and Seyfert 2 galaxies can be well understood by the difference in SEDs of ionizing radiation from the accretion disk. The powerful YRL AGNs favor SED without a strong BBB such as the RIAF, while the line ratios of Seyfert 2 galaxies are consistent with the models adopting SED with a strong BBB (a geometrically thin, optically thick disk). In contrast, the observed difference in the line ratios is difficult to explain by the difference in the contribution of shocks caused by the AGN jets.
2. The line ratio [O III]λ5007/[O III]λ4363 of powerful YRL AGNs is systematically smaller than that of RQ AGNs. If we adopt a scenario that [O III]λ4363 originates in the dense gas clouds, which are located at the inner regions compared with [O III]λ5007, it is inferred that the obscuring torus around powerful YRL AGNs would be thinner than that around Seyfert galaxies.

We thank an anonymous referee for useful and helpful comments. N.K. is financially supported by the Japan Society for the Promotion of Science (JSPS) by the JSPS Research Fellowship for Young Scientists. T.N. is financially supported through the Research Promotion Award of Ehime University. J.W. acknowledges the support provided by NASA through Hubble Fellowship grant HF-0642621 awarded by the Space Telescope Science Institute, which is operated by the Association of Universities for Research in Astronomy, Inc., for NASA, under contract NAS 5-26555.

REFERENCES

Axon, D. J., et al. 2000, AJ, 120, 2284
Balbus, S. A., & Hawley, J. F. 1991, ApJ, 376, 214
Bird, J., Martini, P., & Kaiser, C. 2008, ApJ, 676, 147
Cardelli, J. A., Clayton, G. C., & Mathis, J. S. 1989, ApJ, 345, 245
Chen, X., Abramowicz, M. A., & Lasota, J. P. 1997, ApJ, 476, 61
Dahari, O., & De Robertis, M. M. 1988, ApJ, 331, 727
Dallacasa, D., Stanghellini, C., Centonza, M., & Fanti, R. 2000, A&A, 363, 88
De Zotti, G., & Gaskell, C. M. 1985, A&A, 147, 1
Dopita, M. A., & Sutherland, R. S. 1995, ApJ, 455, 468
Evans, I., Koratkar, A., Allen, M., Dopita, M., & Tsvetanov, Z. 1999, ApJ, 521, 531
Fanti, C., et al. 1995, A&A, 302, 317
Fender, R. P., Belloni, T. M., & Gallo, E. 2004, MNRAS, 355, 1105
Fender, R., et al. 2003, arXiv:astro-ph/0303339
Ferland, G. J. 1997, Hazy: A Brief Introduction to CLOUDY, version 94.00, (Lexington: Univ. Kentucky Dept. Phys. Astron.)
Ferland, G. J., Korista, K. T., Verner, D. A., Ferguson, J. W., Kingdon, J. B., & Verner, E. M. 1998, PASP, 110, 761
Ferland, G. J., & Netzer, H. 1983, ApJ, 264, 105
Frank, J., King, A., & Raine, D. 1992, Accretion Power in Astrophysics, (Cambridge: Cambridge Univ. Press)
Gelderman, R., & Whittle, M. 1994, ApJS, 91, 491
Ghisellini, G., & Celotti, A. 2001, A&A, 379, L1
Giroletti, M. 2007, arXiv:0707.3516
Giroletti, M., et al. 2003, A&A, 339, 889
Grevesse, N., & Sauval, A. J. 1998, Space Sci. Rev., 85, 161
Gugliucci, N. E., Taylor, G. B., Peck, A. B., & Giroletti, M. 2005, ApJ, 622, 136
Gugliucci, N. E., Taylor, G. B., Peck, A. B., & Giroletti, M. 2007, ApJ, 661, 78
Heckman, T. M. 1980, A&A, 87, 152
Ho, L. C. 1999, ApJ, 516, 672
Holt, J., Tadhunter, C. N., & Morganti, R. 2008, MNRAS, 387, 639
Holweger, H. 2001, in AIP Conf. Proc. 598, Joint SOHO/ACE Workshop "Solar and Galactic Composition" ed. R. F. Wimmer Schweingruber, (Mellville, NY: AIP), 23
Homan, J., et al. 2005, ApJ, 624, 295
Kato, S., Fukue, J., & Mineshige, S. 1998, Black-Hole Accretion Disks, (Kyoto: Kyoto Univ. Press)
Kauffmann, G., et al. 2003, MNRAS, 346, 1055
Kawakatu, N., Nagai, H., & Kino, M. 2008, ApJ, 687, 141
Kawakatu, N., & Wada, K. 2008, ApJ, 681, 73
Keel, W. C., & Miller, J. S. 1983, ApJ, 266, L89
Kino, M., Kaburaki, O., & Yamazaki, N. 2000, ApJ, 536, 788
Koski, A. T., & Osterbrock, D. E. 1976, ApJ, 203, L49
Kunert-Bajraszwska, M., Marecki, A., Thomasson, P., & Spencer, R. E. 2005, A&A, 440, 93
Kurpiewski, A., & Jaroszynski, M. 1999, A&A, 346, 713
Labiano, A. 2008, A&A, 488, L59
Labiano, A., et al. 2005, A&A, 436, 493
Laing, R. A., Riley, J. M., & Longair, M. S. 1983, MNRAS, 204, 151
Lawrence, C. R., Zucker, J. R., Readhead, A. C. S., Unwin, S. C., Pearson, T. J., & Xu, W. 1996, ApJS, 107, 541
Lister, M. L., Tingay, S. J., & Preston, R. A. 2001, ApJ, 554, 964
Luo, W.-F., et al. 2007, ChJAA, 7, 611
Machida, M., Hayashi, M. R., & Matsumoto, R. 2000, ApJ, 532, L67
Machida, M., & Matsumoto, R. 2003, ApJ, 585, 429
Manmoto, T. 2000, ApJ, 534, 734
Manmoto, T., Mineshige, S., & Kusunose, M. 1997, ApJ, 489, 791
Marchesini, D., Celotti, A., & Ferrarese, L. 2004, MNRAS, 351, 733
Morganti, R., Tadhunter, C. N., Dickson, R., & Shaw, M. 1997, A&A, 326, 130
Mouri, H., Kawara, K., & Taniguchi, Y. 2000, ApJ, 528, 186
Murayama, T., & Taniguchi, Y. 1998, ApJ, 497, L9
Nagai, H., Inoue, M., Asada, K., Kameno, S., & Doi, A. 2006, ApJ, 648, 148
Nagao, T., Maiolino, R., & Marconi, A. 2006, A&A, 447, 863
Nagao, T., Murayama, T., Shioya, Y., & Taniguchi, Y. 2002, ApJ, 567, 73
Nagao, T., Murayama, T., & Taniguchi, Y. 2001a, ApJ, 546, 744
Nagao, T., Murayama, T., & Taniguchi, Y. 2001b, ApJ, 549, 155
Nagao, T., Taniguchi, Y., & Murayama, T. 2000, AJ, 119, 2605
Nagao, T., Taniguchi, Y., & Murayama, T. 2001c, PASJ, 53, 629
Narayan, R., Kato, S., & Honma, F. 1997, ApJ, 476, 49
Narayan, R., & Yi, I. 1995, ApJ, 444, 231
O'Dea, C. P. 1998, PASP, 110, 493
O'Dea, C. P., & Baum, S. A. 1997, AJ, 113, 148
O'Dea, C. P., et al. 2002, AJ, 123, 2333
Ohsuga, K., Kato, Y., & Mineshige, S. 2005, ApJ, 627, 782
Orienti, M., Dallacasa, D., & Stanghellini, C. 2007, A&A, 475, 813
Osterbrock, D. E. 1989, Astrophysics of Gaseous Nebulae and Active Galactic Nuclei, (Mill Valley, CA: Univ. Sci. Books)
Owsianik, I., Conway, J. E., & Polatidis, A. G. 1998, A&A, 336, 37
Panessa, F., et al. 2006, A&A, 455, 173
Parma, P., Murgia, M., Morganti, R., Capetti, A., de Ruiter, H. R., & Fanti, R. 1999, A&A, 344, 7
Pearson, T. J., & Readhead, A. C. S. 1988, ApJ, 328, 114
Polatidis, A. G., & Conway, J. E. 2003, PASA, 20, 69
Quataert, E., & Narayan, R. 1999, ApJ, 520, 298
Rawlings, S., & Saunders, R. 1991, Nature, 349, 138
Readhead, A. C. S., et al. 1996, ApJ, 460, 634
Remillard, R. A. 2005, arXiv:astro-ph/0504129
Remillard, R. A., & McClintock, J. E. 2006, ARA&A, 44, 49
Rodriguez-Ardila, A., Pastoriza, M. G., & Donzelli, C. J. 2000, ApJS, 327, 63
Rose, J. A., & Cecil, G. 1983, ApJ, 266, 531
Rose, J. A., & Tripicco, M. J. 1984, ApJ, 285, 55
Schmitt, H. R. 1998, ApJ, 506, 647
Shakura, N. I., & Sunyaev, R. A. 1973, A&A, 24, 337
Shuder, J. M., & Osterbrock, D. E. 1981, ApJ, 250, 55
Snellen, I. A. G., Schilizzi, R. T., & van Langevelde, H. J. 2000, MNRAS, 319, 429
Stanghellini, C., O'Dea, C. P., & Murphy, D. W. 1999, A&AS, 134, 309
Tadhunter, C. N., Morganti, R., di Serego-Alighieri, S., Fosbury, R. A. E., & Danziger, I. J. 1993, MNRAS, 263, 999

Taylor, G. B., Marr, J. M., Pearson, T. J., & Readhead, A. C. S. 2000, ApJ, 541, 112
Tschager, W., et al. 2000, A&A, 360, 887
Villar-Martin, M., Tadhunter, C., & Clark, N. 1997, A&A, 323, 21
Wada, K., & Norman, C. A. 2002, ApJ, 566, L21
Wilkinson, P. N., et al. 1994, ApJ, 432, L87
Willott, C. J., Rawlings, S., Blundell, K. M., & Lacy, M. 1999, MNRAS, 309, 1017
Wold, M., Lacy, M., & Armus, L. 2007, A&A, 470, 531
Yee, H. K. C. 1980, ApJ, 241, 894
York, D. G., et al. 2000, AJ, 120, 1579
Yuan, F., Ma, R., & Narayan, R. 2008, ApJ, 679, 984